Modelling the Impact of Patient-Specific Fibrosis and Anatomy on Atrial Fibrillation Triggered by Pulmonary Vein Ectopy

Cynthia Nwanna[1], Laura Bevis[1], Semhar Misghina[1], Caterina Vidal Horrach[1], Ovais Ahmed Jaffery[1], Mahmoud Ehnesh[1], Thomas Iskratsch[1], Andrew Tinker [1], Sherry Honarbakhsh[1] , Caroline Roney[1]

[1]Queen Mary University of London, London, United Kingdom

Abstract

Atrial fibrillation (AF) is sustained by interactions between atrial geometry, fibrosis, and pulmonary vein (PV) ectopy. The combined effects of ectopic timing, patient-specific fibrosis distribution, and anatomical variability on re-entry remain unclear.

We simulated ten patient-specific biatrial geometries under PV ectopy at 160–170 ms using openCARP, with and without fibrotic remodelling. AF inducibility, defined as the proportion of pacing protocols producing sustained re-entry, was analysed alongside anatomical metrics and fibrosis burden.

Inducibility varied across models, with some showing consistently high AF inducibility from PV ectopy and others remaining non-inducible. Larger atrial roofs were associated with higher inducibility, while fibrosis showed weak, non-significant trends (r = –0.38 non-fibrotic; r = 0.27 fibrotic). In some high-fibrosis models, re-entry was stabilised, with phase singularities anchoring to the posterior wall, roof, and PV ostia.

These results suggest that atrial roof size strongly influences AF inducibility, while fibrotic burden can stabilize re-entrant activity. Patient-specific computational models provide mechanistic insight into AF drivers and may guide personalised ablation strategies.

1. Introduction

Atrial fibrillation (AF) is the most common sustained cardiac arrhythmia, characterised by rapid and disorganised electrical impulses that disrupt the normal function of the sinoatrial node [1]. Its prevalence is increasing, particularly among individuals over 65, and AF is associated with significant health risks, including stroke, dementia, and heart failure. Catheter ablation (CA) is widely regarded as the gold standard for treatment, yet challenges remain in predicting optimal ablation targets and preventing recurrence [1]. Pulmonary vein isolation (PVI), the cornerstone of CA, is limited by the complex structural and electrical features of AF, including atrial fibrotic remodelling [2].

Previous work has shown that atrial geometry, including chamber size, wall thickness, and pulmonary vein configuration, modulates conduction pathways and can influence AF inducibility [14,15]. Fibrotic remodelling further alters conduction velocity, promotes re-entrant activity, and is strongly associated with poorer ablation outcomes [2,13,16]. Despite this, the interplay between atrial geometry, fibrotic burden, and ectopic trigger timing on AF inducibility is not fully characterised. Recent advances in computational modelling and patient-specific digital twins provide a powerful platform to address this gap by systematically evaluating structural and electrical contributors to AF [17]. In this study, we use such simulations to assess how atrial geometry and fibrosis influence AF inducibility from pulmonary vein ectopy, aiming to improve mechanistic understanding and inform personalised ablation strategies.

2. Methods

2.1. Patient-Specific Model Generation

Patient-specific bi-atrial models were developed from late gadolinium enhanced (LGE) cardiac magnetic resonance imaging (MRI) data of 10 cases from the STACOM Atrial Segmentation Challenge Dataset (2018) [5]. These models were originally constructed for a previous study from LGE-MRI segmentations using 3D Slicer software. Bilayer atrial models were generated with the atrialmtk pipeline and the Universal Atrial Coordinate system (https://github.com/pcmlab/atrialmtk) [7], incorporating structural and fibre orientation information from the Labarthe et al. (2014) atlas. This included endocardial and epicardial fibres, pectinate muscles, crista terminalis, Bachmann's bundle, the sinoatrial node, and interatrial pathways [10,11].

2.2. Biophysical Modelling

Biophysical simulations were conducted using the

human atrial ionic model developed by Courtemanche et al. (1999) alongside the monodomain solver within openCARP to simulate excitation propagation [8]. To account for persistent AF remodelling and repolarization variability, the ionic model parameters were adjusted following our previous study [6].

2.3. Fibrosis Modelling

To model the effects of fibrotic remodelling, regions of conduction slowing (structural remodelling) were added depending on the LGE-MRI image intensity ratio. A fibrosis map was generated by superimposing the bi-atrial surface mesh on the scan data and computing the maximum intensity projection of voxels along the normal direction of each surface element [9]. This allowed projection of the image intensity ratio (IIR) onto the mesh, facilitating identification of fibrosis. Tissue-level conductivities were then modified according to IIR thresholds as follows: IIR < 0.9: 0.4 S/m (CV: 0.81 m/s), 0.9 < IIR < 1.4: 0.31 S/m (CV: 0.74 m/s) 1.4 < IIR < 1.6: 0.28 S/m (CV: 0.71 m/s), 1.6 < IIR: 0.19 S/m (CV: 0.58 m/s) [9].

2.4. Pacing Protocol to Test Inducibility

Arrhythmia inducibility was assessed using extra stimulus pacing of the right superior pulmonary vein (RSPV) and the left superior pulmonary vein (LSPV). The RSPV was paced with five beats, while the LSPV received ten beats. Simulations were conducted to evaluate the effects of simultaneous ectopic activity on inducibility. To investigate likelihood of AF induction from PV ectopics, pacing was performed at three different cycle lengths per model setup: 160ms, 165ms and 170 ms. Inducibility was measured as the proportion of cycle lengths resulting in re-entry, referred to as the inducibility ratio.

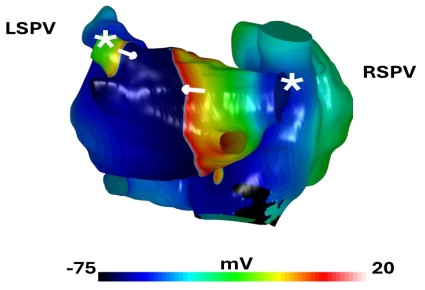

Figure 1. Transmembrane map of pacing protocol. Simulated activation map in a biatrial model (case M24) showing sequential pacing in the left atrium (LA) (*). Pacing was applied first at the right superior pulmonary vein (RSPV) and then at the left superior pulmonary vein (LSPV) 100 ms later, producing a right-to-left activation wave across the LA (arrows).

2.5. Metrics & Post-Processing

Several anatomical and electrophysiological metrics were quantified. Anatomical landmarks were identified using a point-picking tool to measure atrial roof length, left and right pulmonary vein (PV) diameters, and posterior wall length, with distances calculated in MATLAB. Fibrosis burden was calculated as the percentage of atrial surface area classified as fibrotic relative to the total bi-atrial surface area. Arrhythmia dynamics were assessed using the AF inducibility ratio (proportion of pacing sites that induced sustained AF) and AF maintenance (duration of sustained AF episodes up to 10 s). For cases sustaining AF, phase singularity (PS) metrics were calculated, including total counts, spatial density maps, hotspot localisation, and variability in rotor activity.

Phase singularities (PSs) were detected over 10 s of arrhythmia data, or until AF terminated, to identify centres of rotational activity and re-entrant drivers. PSs were post-processed to generate spatial density maps, and total PS counts, hotspots, and variations in rotor activity were quantified [12]. Statistical associations between anatomical features, fibrosis burden, and AF inducibility ratios were evaluated using the Pearson correlation coefficient in R, where 1 indicates a perfect positive linear correlation, 0 indicates no linear correlation, and −1 indicates a perfect negative correlation.

3. Results

3.1. AF Inducibility Ratio Varies Across Patient-Specific Anatomical Models

AF inducibility differed substantially across 10 patient-specific non-fibrotic left atria at the tested cycle lengths (160, 165, and 170 ms). Two atria (M24, M44) were inducible at all cycle lengths, whereas three atria (M9, M10, M15) were never inducible, highlighting distinct high and low responder phenotypes.

3.2. Anatomical Effects on AF Inducibility

We also investigated the influence of atrial anatomical features on AF susceptibility. Left and right pulmonary vein (PV) diameters and posterior wall size showed no consistent association with inducibility. In contrast, atrial roof dimension was a strong determinant of AF vulnerability. Models with larger roof dimensions were consistently inducible, whereas smaller roofs remained non-inducible. For instance, M44, with the largest roof size (43.8 mm), demonstrated sustained re-entry anchored near the roof and left inducible under identical pacing conditions (Fig. 2B). In fibrotic models, roof dimension correlated positively with inducibility ratio (Pearson r =

0.70, p = 0.025), supporting a role for anatomical factors in modulating AF susceptibility.

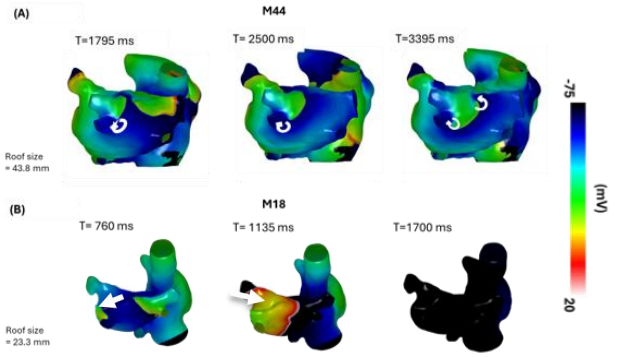

Figure 2. Effect of LA roof size on AF dynamics. Transmembrane potential maps from openCARP simulations at multiple time points following pacing. (A) Largest LA roof (43.8 mm) exhibits sustained rotational activity (curved arrows). (B) Smallest LA roof (23.3 mm): no re-entry (straight arrows).

3.3. Effects of Atrial Fibrosis on AF Inducibility and Re-Entry Dynamics

Fibrosis increased AF inducibility (mean ratio 0.40 in non-fibrotic vs. 0.58 in fibrotic models), though effects were case-dependent (Table 1, Fig. 3A). M9, with the highest fibrosis burden (53.6%), and M10 (11% fibrosis) transitioned from non-inducible to inducible, whereas other models with moderate fibrosis remained non-inducible.

Phase singularity (PS) mapping in M9 confirmed that fibrosis stabilised re-entrant activity, with hotspots localised to the posterior wall, roof, and pulmonary vein ostia, suggesting potential anchoring sites for sustained rotor activity (Fig. 3B–D). Non-fibrotic M9 exhibited AF termination with no persistent hotspots (Fig. 3B),

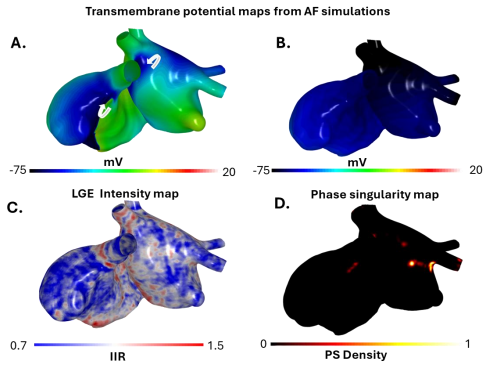

Figure 3. Effects of fibrosis on AF dynamics in M9, the model with the largest fibrosis burden. (A–B) Rotational activity with fibrosis (A) versus AF termination without fibrosis (B). (C) Fibrosis distribution from LGE-MRI. (D) PS density map (fibrosis), with hotspots showing re-entrant activity localized to the pulmonary vein ostia, posterior wall, and roof.

indicating that fibrosis can provide spatial support for re-entry. Correlation analysis showed a weak negative association between fibrosis burden and inducibility in non-fibrotic models (Pearson r = –0.38) and a positive trend in fibrotic models (Pearson r = 0.27).

4. Discussion

In this study, we investigated how patient-specific atrial anatomy and fibrosis patterns influence AF inducibility and rotor dynamics. Our findings indicate that larger atrial roofs support sustained re-entry, whereas smaller roofs were generally non-inducible, likely due to limited wavefront curvature and limited space for wavefront propagation. While prior studies have linked pulmonary vein size to AF susceptibility [9], we observed no clear association in our cohort, highlighting the importance of considering structural heterogeneity beyond conventional PV-focused assessments.

Fibrotic remodelling further shaped re-entrant activity, providing anchoring sites in the posterior wall, roof, and PV ostia, as demonstrated by phase singularity mapping. The effects of fibrosis were case-dependent: moderate fibrosis stabilised re-entry, while very high fibrosis sometimes prevented rotor maintenance. These observations extend prior computational and clinical studies [12], showing that the spatial distribution of fibrosis, rather than total burden, is the critical determinant of rotor localisation and AF persistence. In atria with higher fibrosis burden, rotors preferentially anchored to scarred regions, whereas lower-burden atria exhibited rotor activity near anatomical features such as PV ostia.

Our results have potential clinical implications. Pre-ablation imaging of atrial geometry and fibrosis distribution could help identify patient-specific regions prone to sustained re-entry, offering targets for personalised ablation strategies beyond standard PV isolation. This approach complements prior studies that have tailored ablation strategies using structural and fibrotic imaging data [12,14] and may be particularly valuable in patients with complex atrial substrates.

Several factors limit the interpretation of our results. Fibrosis modelling was based on LGE-MRI intensity thresholds, which may oversimplify tissue heterogeneity, and the bilayer atrial representation does not capture full transmural conduction. Short pacing protocols and the absence of lesion delivery further limit replication of long-term AF maintenance or ablation outcomes.

Future work should develop fully volumetric atrial models incorporating realistic conduction dynamics, patient-specific electrophysiology, and ablation effects. Integrating high-resolution imaging and longitudinal ECG data could identify regions most likely to sustain AF, particularly where anatomical features and fibrosis interact. This approach supports personalised ablation

Table 1. AF inducibility ratios and fibrosis burden across patient-specific atrial models. Inducibility ratio = proportion of pacing protocols resulting in AF. Inducibility outcome defined as (0 = non-inducible, AF terminated; 1 = inducible.

Parameter	M9	M10	M11	M15	M18	M20	M23	M24	M44	M45	Average
Roof dimension (mm)	33.6	27.2	30.9	23.9	23.3	23.9	27.5	27.7	42.8	28.0	—
Non-fibrotic inducibility ratio	0.0	0.0	0.7	0.0	0.0	0.3	0.3	1.0	1.0	0.7	0.40
Fibrotic inducibility ratio	0.7	0.7	0.7	0.3	0.0	0.7	0.3	0.7	1.0	0.7	0.58
Fibrosis (%)	53.6	11.0	11.7	5.0	19.1	27.8	6.5	30.2	12.8	25.1	—

strategies tailored to each patient's atrial structure, ultimately improving treatment outcomes.

Our study demonstrates that patient-specific atrial geometry and the spatial distribution of fibrosis jointly shape AF dynamics. These findings highlight the potential of integrating high-resolution imaging with computational simulations to predict AF inducibility and inform personalised ablation strategies, advancing patient-specific AF management.

Acknowledgments

This research was funded by a UKRI Future Leaders Fellowship (MR/W004720/1) and a British Heart Foundation PhD studentship.

References

[1] The Lancet Regional Health, "Atrial Fibrillation 2024", 2024, URL https://www.thelancet.com/series-do/europe-atrial-fibrillation.

[2] L. Zhang *et al.*, "Health-related quality of life in atrial fibrillation patients over 65 years: A review," *Eur J Prev Cardiol*, vol. 22, no. 8, pp. 987–1002, Jun. 2014.

[3] C. H. Roney *et al.*, "Variability in pulmonary vein electrophysiology and fibrosis determines arrhythmia susceptibility and dynamics," *PLoS Comput Biol.*, vol. 14, e1006166, May. 2018.

[4] A. Roy *et al.*, "Identifying locations of re-entrant drivers from patient-specific distribution of fibrosis in the left atrium," *PLoS Comput Biol.*, vol. 16, no. 9, pp. e1008086–e1008086, Sep. 2020.

[5] Z. Xiong *et al.*, "A global benchmark of algorithms for segmenting the left atrium from late gadolinium-enhanced cardiac magnetic resonance imaging," *Med Image Anal*, vol. 67, p. 101832, Jan. 2021.

[6] J. D. Bayer *et al.*, "Novel Radiofrequency Ablation Strategies for Terminating Atrial Fibrillation in the Left Atrium: A Simulation Study," *Front Physiol*, vol. 7, Apr. 2016.

[7] C. H. Roney *et al.*, "Constructing bilayer and volumetric atrial models at scale," *Interface Focus*, vol. 13, no. 6, Dec. 2023.

[8] M. Courtemanche, "Ionic targets for drug therapy and atrial fibrillation-induced electrical remodeling: insights from a mathematical model," *Cardiovasc Res*, vol. 42, no. 2, pp. 477–489, May. 1999.

[9] José Alonso Solís-Lemus *et al.*, "Evaluation of an open-source pipeline to create patient-specific left atrial models: A reproducibility study," *Comput Biol Med*, vol. 162, pp. 107009–107009, Aug. 2023.

[10] C. H. Roney *et al.*, "Universal atrial coordinates applied to visualisation, registration and construction of patient specific meshes," *Med Image Anal*, vol. 55, pp. 65–75, Jul. 2019.

[11] X. Zhuang *et al.,* "A registration-based propagation framework for automatic whole heart segmentation of cardiac MRI," *IEEE Trans Med Imaging*, vol. 29, no. 9, pp. 1612–1625, Sep. 2010.

[12] C. H. Roney *et al.*, "Predicting Atrial Fibrillation Recurrence by Combining Population Data and Virtual Cohorts of Patient-Specific Left Atrial Models," *Circ Arrhythm Electrophysiol*, vol. 15, no. 2, Feb. 2022.

[13] N. F. Marrouche *et al.*, "Association of Atrial Tissue Fibrosis Identified by Delayed Enhancement MRI and Atrial Fibrillation Catheter Ablation," *JAMA*, vol. 311, no. 5, pp. 498–498, Feb. 2014.

[14] J. Zhao *et al.*, "Three-dimensional Integrated Functional, Structural, and Computational Mapping to Define the Structural 'Fingerprints' of Heart-Specific Atrial Fibrillation Drivers in Human Heart Ex Vivo," *J Am Heart Assoc*, vol. 6, no. 8, Aug. 2017.

[15] S. Zahid *et al.*, "Patient-derived models link re-entrant driver localization in atrial fibrillation to fibrosis spatial pattern," *Cardiovasc Res*, vol. 110, no. 3, pp. 443–454, Jun. 2016.

[16] H. Cochet *et al.*, "Relationship Between Fibrosis Detected on Late Gadolinium-Enhanced Cardiac Magnetic Resonance and Re-Entrant Activity Assessed With Electrocardiographic Imaging in Human Persistent Atrial Fibrillation," *JACC. Clin Electrophysiol*, vol. 4, no. 1, pp. 17–29, Nov. 2017.

[17] P. Bhagirath *et al.,* "From bits to bedside: entering the age of digital twins in cardiac electrophysiology," *EP Europace*, vol. 26, no. 12, Dec. 2024.

Address for correspondence:

Cynthia Nwanna
Queen Mary University of London, UK
c.nwanna@se17.qmul.ac.uk